

1 **Proteomic profiling reveals roles of stress response, Ca²⁺ transient dysregulation and novel signaling**
2 **pathways in alcohol-induced cardiotoxicity**

3

4 Rui Liu^{1,2}, Fangxu Sun³, Parvin Forghani¹, Lawrence C. Armand¹, Antonio Rampoldi¹, Dong Li¹, Ronghu
5 Wu³, and Chunhui Xu^{1,4,*}

6

7 ¹Department of Pediatrics, Emory University School of Medicine and Children's Healthcare of Atlanta,
8 Atlanta, GA 30322, USA

9 ²Department of Pediatrics, the Third Xiangya Hospital of Central South University, Changsha, Hunan
10 410013, China

11 ³School of Chemistry and Biochemistry and the Petit Institute for Bioengineering and Bioscience, Georgia
12 Institute of Technology, Atlanta, GA 30332, USA

13 ⁴Wallace H. Coulter Department of Biomedical Engineering, Georgia Institute of Technology and Emory
14 University, Atlanta, GA 30322, USA

15

16 *Correspondence:

17 Chunhui Xu, PhD, Associate Professor, Department of Pediatrics, Emory University School of Medicine,
18 2015 Uppergate Drive, Atlanta, GA 30322. Email: chunhui.xu@emory.edu

19

20 Abstract

21 **Background:** Alcohol use in pregnancy increases the risk of abnormal cardiac development, and excessive
22 alcohol consumption in adults can induce cardiomyopathy, contractile dysfunction, and arrhythmias.
23 Understanding molecular mechanisms underlying alcohol-induced cardiac toxicity could provide guidance
24 in the development of therapeutic strategies.

25 **Methods:** We have performed proteomic and bioinformatic analysis to examine protein alterations globally
26 and quantitatively in cardiomyocytes derived from human pluripotent stem cells (hiPSC-CMs) treated with
27 ethanol. Proteins in both cell lysates and extracellular culture media were systematically quantitated.

28 **Results:** Treatment with ethanol caused severe detrimental effects on hiPSC-CMs as indicated by
29 significant cell death and deranged Ca^{2+} handling. Treatment of hiPSC-CMs with ethanol significantly
30 affected proteins responsible for stress response (e.g. GPX1 and HSPs), ion channel related proteins (e.g.
31 ATP1A2), myofibril structure proteins (e.g. MYL2/3), and those involved in focal adhesion and
32 extracellular matrix (e.g. ILK and PXN). Proteins involved in the TRAF2 signaling (e.g. CPNE1 and TNIK)
33 were also affected by ethanol treatment.

34 **Conclusions:** The observed changes in protein expression highlight the involvement of oxidative stress and
35 dysregulation of Ca^{2+} handling and contraction while also implicating potential novel targets in alcohol-
36 induced cardiotoxicity. These findings facilitate further exploration of potential mechanisms, discovery of
37 novel biomarkers, and development of targeted therapeutics against ethanol-induced cardiotoxicity.

38

39 **Keywords**

40 Stem cells, cardiomyocytes, cardiotoxicity, ethanol, quantitative proteomics

INTRODUCTION

41
42
43
44
45
46
47
48
49
50
51
52
53
54
55
56
57
58
59
60
61
62
63
64
65
66

Excessive alcohol consumption continues to be a major cause of mortality and morbidity in the US and the relevance of alcohol abuse for public health is well established (GBD 2016 Alcohol Collaborators, 2018; White et al., 2020). In a recent study, the National Institute on Alcohol Abuse and Alcoholism (NIAAA) reported that nearly 1 million people died from alcohol-related causes between 1999 and 2017 and that in 2017 alcohol played a role in 2.6% of all deaths in the US (White et al., 2020). Excessive alcohol consumption is known to elicit adverse effects on multiple organs and systems, including the heart.

With respect to the heart, alcohol can induce cardiomyopathy, contractile dysfunction and arrhythmias, leading to heart failure, myocardial infarction (MI), and sudden cardiac death (Whitman et al., 2017). Heavy alcohol consumption in a binge pattern can cause an acute cardiac rhythm and/or conduction disturbance even in those with normal heart function. In this type of severe arrhythmia, atrial fibrillation is the most common, followed by atrial flutter, junctional tachycardia, premature ventricular and atrial complexes, paroxysmal atrial tachycardia, and ventricular tachycardia (Day and Rudd, 2019). In addition, alcohol exposure during pregnancy is known to disrupt fetal development and increase the risk of fetal alcohol spectrum disorder (FASD) (Roozen et al., 2016). Nearly 1 out of 3 FASD children are diagnosed with congenital heart defects and each year there are approximately 10,000 cases of alcohol-induced congenital heart defects in the US, indicating that parental alcohol consumption confers detriment effect on cardiac development in a large number of the children (Zhang et al., 2020). Unfortunately, without effective therapies further heart complications may develop later in life.

Understanding pathophysiological mechanisms underlying alcohol-induced cardiac toxicity could provide guidance in the development of therapeutic strategies. Studies in several model systems have provided significant insights into the mechanisms of ethanol-induced damage to cardiomyocyte (CM) (Tan et al., 2012; Guo et al., 2012; Maiuolo et al., 2018). For instance, oxidative stress mediated mitochondria dysfunction was found to contribute to alcohol-induced heart failure in mice (Brandt et al., 2016). Sarcoplasmic reticulum Ca^{2+} -leak and disordered excitation-contraction coupling were found to play an important role in the arrhythmogenic effects of ethanol on murine and human CMs (Mustroph et al., 2018).

67 More recently, human induced pluripotent stem cell-derived cardiomyocytes (hiPSC-CMs) have been used
68 to study alcohol-induced cardiotoxicity (Rampoldi et al., 2019)—hiPSC-CMs are a physiologically relevant
69 model to human fetal cardiomyocytes because of their immature nature and they can overcome the
70 limitations of human primary CM samples which are difficult to acquire and maintain *in vitro* (Pinheiro et
71 al., 2019). In this model, treatment of the cells dose-dependently increased the production of reactive
72 oxygen species, cell death, and abnormal Ca²⁺ transients and CM contraction (Rampoldi et al., 2019).

73 Comparative gene expression profiling could help uncover genes and pathways that play important
74 roles in disease processes. Previous studies have provided data on transcriptome alterations in ethanol-
75 induced cardiotoxicity (Rampoldi et al., 2019). However, global protein changes upon the treatment of the
76 CMs with ethanol have not been reported. Modern mass spectrometry (MS)-based proteomics technique
77 enables global protein identification and quantification in complex biological samples (Xiao et al., 2015;
78 Aebersold and Mann, 2016; Mann, 2016; Orlando and Aebersold, 2019), and it has been employed to
79 unmask molecular mechanisms such as doxorubicin-induced cardiotoxicity, dilated cardiomyopathy, and
80 MI (Isserlin et al., 2010; Peng et al., 2014; Tomlinson et al., 2019).

81 In this study, we have performed proteomic analysis to examine protein alterations globally and
82 quantitatively in hiPSC-CMs treated with ethanol. Proteins in both cell lysates and extracellular culture
83 media were systematically quantitated. Here we report the proteins with significant changes caused by
84 ethanol treatment as well as the biological processes and pathways associated with the affected proteins.
85 These proteins are involved in stress response, ion channels, myofibril structure, focal adhesion, and
86 extracellular matrix (ECM). Our study also reveals other novel targets including TNF receptor-associated
87 factor 2 (TRAF2) signaling in alcohol-induced cardiotoxicity. We provide a unique resource: a human
88 proteomic dataset for ethanol-induced cardiotoxicity that aids in a better understanding of the molecular
89 mechanisms of the alcohol-induced cardiotoxicity.

90

91

MATERIALS AND METHODS

92

93 *Culture of hiPSCs and cardiomyocyte differentiation*

94 Undifferentiated hiPSCs (SCVI-273 line, obtained from Stanford Cardiovascular Institute) were
95 fed daily on Matrigel-coated plates with mTeSR™ medium and passaged using Versene when compact
96 colonies reached 90% confluence. For CM differentiation, hiPSCs were induced using a small molecule-
97 guided differentiation protocol (BurrIDGE et al., 2014). At the day of induction (day 0), medium was replaced
98 with RPMI 1640 medium supplemented with 2% B27 minus insulin containing 6 μM CHIR99021. After
99 induction for 48 h, the medium was replaced with RPMI supplemented with 2% B27 minus insulin. After
100 another 24 h, the medium was replaced with fresh RPMI supplemented with 2% B27 minus insulin
101 containing 5 μM IWR1. After a further 48 h, the medium was replaced with RPMI supplemented with 2%
102 B27 with insulin. At day 6, the cells were dissociated and re-seeded into AggreWell™400 plates to acquire
103 cardiospheres (CSs) (Jha et al., 2016). After 24 h, the CSs formed were transferred to low-adhesion dishes
104 for suspension culture. The medium was changed every other day. CSs typically started beating
105 spontaneously by day 8 to 10. Information about the vendors and catalog numbers for major reagents are
106 included in Table S1.

107

108 *Immunocytochemistry*

109 For the immunocytochemical staining, differentiation cultures were dissociated and reseeded onto
110 96-well plates. Cells were fixed in 4% paraformaldehyde for 15 min and permeabilized using ice-cold
111 methanol for 2 min at room temperature (RT). The cells were then incubated with 5% normal goat serum
112 (NGS) in phosphate-buffered saline (PBS) at RT for 1 h and then incubated with primary antibodies (Table
113 S2) in 3% NGS overnight at 4°C. After washing, the cells were incubated with the corresponding secondary
114 antibodies at RT for 1 h in dark followed by counterstaining the nuclei with 7 μM Hoechst33342. Imaging
115 was performed using an inverted microscope (Axio Vert.A1).

116

117 *Cardiomyocyte purity assay*

118 Differentiation cultures were analyzed for CM purity using antibodies against NKX2-5, a cardiac
119 specific transcription factor. Following immunocytochemistry, images of Hoechst and NKX2-5-positive
120 cells were acquired and quantitatively analyzed using ArrayScan™ XTI Live High Content Platform
121 (Thermo Fisher Scientific). Acquisition Software Cellomics Scan was used to capture images via a 10×
122 objective camera. Each well was sectioned to 7×7 fields in total and 20 fields in the center were selected.
123 Images were analyzed using Cellomics View Software with mask modifiers for Hoechst and NKX2-5
124 restricted to the nucleus. The percentage of cells positive for NKX2-5 was calculated as CM purity
125 (Rampoldi et al., 2019).

126

127 *Ethanol treatment*

128 For the ethanol treatment experiments, a working solution of 200 mM ethanol was freshly prepared
129 by diluting pure ethyl alcohol in the culture medium. Prior to ethanol treatment, medium in cell culture
130 wells was replaced with 1 volume of medium. An equal volume of the 200 mM ethanol working solution
131 was then added to the wells. The final concentration of ethanol in the cell culture was 100 mM. Mineral oil
132 was overlaid on top of the medium to prevent ethanol evaporation. In addition, ethanol-containing medium
133 was refreshed every other day.

134

135 *Cell viability assay*

136 Cell viability was measured using the CellTiter-Blue® Cell Viability Assay, which is a fluorometric
137 method for estimating the number of viable cells based on the metabolic capacity of cells. On the day of
138 analyzing cell viability, CellTiter-Blue reagent was added into culture wells at a ratio of 1:5 to the medium,
139 and the plates were incubated for 2 to 4 h at 37°C in dark. After the incubation, fluorescence was measured
140 using the Synergy 2 Microplate Reader (BioTek) and Gen5 3.03 Microplate Reader and Imager Software
141 with an excitation wavelength of 530 nm and an emission wavelength of 590 nm.

142

143 *Ca²⁺ transient assay*

144 Live cell imaging of intracellular Ca^{2+} transients was performed using cell permeant dye Fluo-4
145 AM. hiPSC-CMs at a low density were incubated with $5\mu\text{M}$ Fluo-4 AM for 30 min at 37°C in dark followed
146 by a 5 min wash with warm $1\times$ normal Tyrode solution (148 mM NaCl, 4 mM KCl, 0.5 mM $\text{MgCl}_2\cdot 6\text{H}_2\text{O}$,
147 0.3 mM $\text{NaPH}_2\text{O}_4\cdot\text{H}_2\text{O}$, 5 mM HEPES, 10 mM D-Glucose, 1.8 mM $\text{CaCl}_2\cdot\text{H}_2\text{O}$, pH adjusted to 7.4 with
148 NaOH). Fluorescent images were recorded using the ImageXpress Micro XLS System (Molecular Devices)
149 at a frequency of 5 Hz for 12-32 s with $20\times$ magnification. The fluorescence intensities over time for
150 individual cells were analyzed through MetaXpress software (Molecular Devices) by measurements in the
151 region of interest.

152

153 *Proteomic analysis*

154 *Cell lysis and protein digestion.* Proteins were extracted from $3\sim 4\times 10^6$ hiPSC-CMs per sample by
155 suspending the cells in the lysis buffer (50 mM HEPES pH = 7.4, 150 mM NaCl, 0.5% SDC, 10 units/mL
156 benzonase, and 1 tablet/10 mL protease inhibitor) at 4°C for 45 min. Protein concentration was determined
157 by the BCA assay, and proteins in all samples were then normalized based on their measured concentrations.
158 Proteins were reduced with 5 mM DTT (56°C , 30 min), followed by alkylation with 14 mM iodoacetamide
159 (RT, 30 min in the dark). They were purified through methanol-chloroform protein precipitation. For
160 secretome analysis, the media was first passed through a filter ($0.45\ \mu\text{m}$) and then concentrated by
161 centrifugation (3 kDa cutoff). The other steps were the same as described for cell lysates. The isolated
162 proteins were digested with trypsin in a buffer containing 50 mM HEPES (pH 8.5), 1.6 M urea at 37°C
163 overnight. After the digestion, peptides were purified using tC18 Sep-Pak cartridges.

164 *TMT labeling and fractionation.* Purified peptides from each sample were labeled with each
165 channel of the six-plexed tandem mass tag (TMT) reagents according to the manufacturer's protocol. The
166 labeled peptides from all six samples were combined and desalted using a tC18 Sep-Pak cartridge. For
167 peptides from the cell lysates, they were further separated into 20 fractions by high pH reversed-phase high-
168 performance liquid chromatography (HPLC) using a 40 min gradient of 5–55% ACN in 10 mM ammonium

169 acetate (pH = 10). Each fraction was purified again by the stage tip method. For secretome analysis, peptides
170 were separated into six fractions during the stage tip.

171 *LC-MS/MS.* Purified and dried peptide samples were dissolved in the loading buffer (5% ACN and
172 4% formic acid), and 2 μ l was injected onto a microcapillary column packed with C18 beads using a WPS-
173 3000TPLRS autosampler (UltiMate 3000). After being separated by reversed-phase HPLC, eluted peptides
174 were directly detected in a hybrid dual-cell quadrupole linear ion trap-orbitrap mass spectrometer (LTQ
175 Orbitrap Elite, Thermo Scientific) using a data-dependent Top15 method. Full MS scan (resolution: 60,000)
176 was recorded in the Orbitrap at 10^6 AGC target. Peptides were fragmented using higher-energy collision
177 dissociation (HCD) with 40% normalized energy and then fragments were detected in the Orbitrap cell with
178 high resolution and high mass accuracy. Ions with a single or unassigned charge were excluded for further
179 sequencing.

180 *Database search, data filtering and quantification.* The raw files were converted to an mzXML
181 format and then searched against the database containing sequences of all human proteins (*Homo sapiens*)
182 downloaded from the UniProt with the SEQUEST algorithm (version 28) (Eng et al., 1994). The following
183 parameters were used during the search: 20 ppm precursor mass tolerance; 0.025 Da product ion mass
184 tolerance; fully digested with trypsin; up to three missed cleavages; fixed modifications:
185 carbamidomethylation of cysteine (+57.0214); TMT tag of lysine (+229.1629) and peptide N-terminus
186 (+229.1629); variable modifications: oxidation of methionine (+15.9949). The target-decoy method was
187 used to evaluate the false discovery rates (FDRs) of peptide and protein identifications, and linear
188 discriminant analysis (LDA), which integrates several parameters including XCorr, precursor mass error,
189 and charge state, was employed to control the quality of peptide identifications (Elias and Gygi, 2007; Kall
190 et al., 2007). Peptides with fewer than seven amino acid residues were removed. Peptide spectral matches
191 and proteins were both filtered to be <1% FDR. The TMT reporter ion intensities in the tandem mass spectra
192 were used to quantify identified peptides and the TMT intensity for one protein was calculated from the
193 median TMT intensity of all peptides from this protein.

194

195 *Bioinformatic analysis*

196 Differentially expressed proteins were recognized when the abundance changed by >1.3-fold
197 ($\log_2(1.3) = 0.38$) compared to the control group and the *P*-value was <0.05. Herein *P*-values were
198 calculated using Perseus (Tyanova et al., 2016), in which a one-sample *t*-test ($S_0 = 0$) was performed. This
199 threshold allowed the selection of a larger number of differentially expressed proteins than if more
200 stringent threshold was used for a broad GO-term and pathway analyses, which should be taken
201 into consideration in the interpretation of these analyses although protein changes at this threshold
202 could have significant biological consequence. Protein functional annotation including Gene Ontology
203 (GO) analysis and KEGG pathway analysis was performed with Database for Annotation, Visualization
204 and Integrated Discovery (DAVID) (Huang et al., 2008). Protein network was constructed through STRING
205 database (interaction score ≥ 0.7) and visualized by Cytoscape (Szklarczyk et al., 2014; Shannon et al.,
206 2003).

207

208 *Statistical methods*

209 Data were analyzed in Excel or R and graphed in GraphPad Prism 7.04 or OriginPro 2020. Data
210 were presented as mean \pm SD. Comparisons were conducted via Student's *t*-test or two-sided Chi-square
211 test with significant differences defined by $P < 0.05$ (*), $P < 0.01$ (**), $P < 0.001$ (***), $P < 0.0001$ (****).
212 Sample sizes were given for each experiment.

213

214 *Proteomics datasets*

215 Proteomics datasets from this study can be found on the PeptideAtlas (Identifier: PASS01620;
216 Password: CY5836iy).

217

218

RESULTS

219

220 *Ethanol treatment induces hiPSC-CM death and Ca²⁺ handling defect*

221 Ethanol treatment induces cardiotoxicity in hiPSC-CMs at the cellular and functional levels
222 (Rampoldi et al., 2019). To further understand ethanol-induced changes in proteins and biological processes,
223 we first generated enriched hiPSC-CMs and treated them with 0 and 100 mM of ethanol for 5 days as we
224 previously reported (Rampoldi et al., 2019) (Fig. 1A, Fig. S1). The concentration of 100 mM ethanol
225 corresponds to the blood alcohol level of ~6 times legally permissible limits and causes confusion. As
226 shown in Fig. 1B, based on CellTiter-Blue Cell Viability Assay, cell viability decreased by 20% when cells
227 were treated with ethanol compared with untreated control.

228 We also assessed the effect of ethanol treatment on the intracellular Ca²⁺ transients in hiPSC-CMs,
229 a critical index of CM function since Ca²⁺ acts as a bridge between electrical excitation and mechanical
230 contraction. We counted the numbers of cells exhibiting normal or abnormal Ca²⁺ transients and calculated
231 the proportion of each category for each culture condition according to the following criteria. Specifically,
232 cells were categorized as normal if the Ca²⁺ transients had mostly consistent amplitudes and rhythmicity,
233 typical cardiac Ca²⁺ transient morphology (i.e. rapid upstroke and decay kinetics), and no obvious
234 spontaneous Ca²⁺ release between transients (Fig. 1C-i). Cells were categorized as abnormal if they
235 exhibited sluggish upstroke or decay morphology (Fig. 1C-ii), oscillations of the diastolic Ca²⁺ signal (Fig.
236 1C-iii and Fig. 1C-iv), unrecognizable single transient morphology (Fig. 1C-v), or notable inconsistent
237 amplitudes or beat periods (Fig. 1C-vi). In the control group, the majority of the cells exhibited normal Ca²⁺
238 transients, whereas in hiPSC-CMs treated with ethanol the percentage of cells exhibiting abnormal Ca²⁺
239 transients increased to 69% (Fig. 1D). In addition, among the observed abnormal Ca²⁺ transients, only two
240 types occurred in the control group (type iv: 33.3%, type vi: 66.7%) , whereas all the five were observed in
241 the treatment group types (type ii: 6.8%, type iii: 16.9%, type iv: 57.6%, type vi: 6.8%, type vi: 11.9%)
242 (Fig. 1D). These observations indicate that exposure of hiPSC-CMs to ethanol results in cell death and
243 dysfunction of intracellular Ca²⁺ handling.

244

245 *Proteomic analysis identifies differentially expressed proteins caused by ethanol treatment*

246 To characterize protein expression changes caused by ethanol treatment, we collected cell lysates
247 and culture media separately from the triplicates of hiPSC-CM 3D-cultures that had been treated with 0
248 mM or 100 mM ethanol for 5 days. After protein extraction and digestion, peptides were labeled with the
249 TMT reagents for protein quantitation. The TMT-labeled samples (6 for cell lysates and 6 for media) were
250 then mixed and fractionated. Each fraction was analyzed by an online LC-MS system. In total, we detected
251 4,538 proteins in the cell lysate samples and 384 proteins in the media samples. The experimental procedure
252 is shown in Fig. 2A.

253 To examine the reproducibility of the biological triplicates, we calculated pairwise Pearson's
254 correlation coefficients for quantitated proteins among the triplicated cell lysate samples. As shown in Fig.
255 2B, the Pearson's correlation coefficients were high for all comparisons within the ethanol-treated group
256 and within the control group, suggesting high reproducibility among the triplicates in each group.

257 To identify proteins affected by ethanol treatment, we systematically quantitated proteins in
258 ethanol-treated and untreated cells. In the cell lysate samples, 201 proteins were found to be significantly
259 different between the ethanol-treated group and the control group ($P < 0.05$, fold change > 1.3 ; see Fig. 2C).
260 Among the 201 differentially expressed proteins, 3 proteins (BST2, CORIN, and VTN) were up-regulated
261 and 198 protein were down-regulated in the ethanol-treated group compared with the control group (Fig.
262 2C). Table 1 lists the top 30 differentially expressed proteins including 3 up-regulated and 27 down-
263 regulated ones. Among them, 7 were related to muscle system process (CRYAB, FLNA, SORBS2, MYL2,
264 ANXA6, HSPB6, and SLMAP) and 13 involved in focal adhesion (VTN, CD59, FLNA, XIRP1, SORBS2,
265 FHL1, AJUBA, FERMT2, LMO7, NEXN, ANXA6, SH3KBP1, and MYL2). Several proteins associated
266 with the TNF receptor-associated factor 2 (TRAF2) pathway were among the significantly down-regulated
267 proteins: CPNE1 (Table 1) and TNIK (expression was reduced by ethanol treatment to 73% of the untreated
268 control, $P = 0.0015$).

269 In the media samples, 5 proteins were found to be significantly different in their levels between the
270 ethanol-treated group and the control group (Fig. 2C). Among the 5 differentially expressed proteins, 4

271 proteins (BANF1, S100A13, RPS21, and HSPB1) were up-regulated and one (VADC1) was down-
272 regulated in the ethanol-treated group compared with the control group (Fig. 2C).

273 To help evaluate if ethanol treatment indeed caused changes of protein levels in cell lysates, we
274 examined whether ethanol treatment also caused changes in the RNA level of the corresponding genes. As
275 shown in Fig. 2D, the mRNA level of BST2 was upregulated in ethanol-treated hiPSC-CMs based on an
276 RNA-Seq analysis (data available at GEO database, Accession: GSE125917 (Rampoldi et al., 2019)) (fold
277 change = 1.31, P -value = 0.0096), which was consistent with the proteomic analysis in this study (fold
278 change = 1.42, P -value = 0.0030). Several other differentially expressed proteins were also found to be
279 differentially expressed at the RNA level (Fig 2D), including those involved in focal adhesion (*FHLL1*,
280 *MCAM*, *AJUBA*, and *ZYX*) and relevant to myofibril (*CSRFP3*, *MYOZ2*, *CRYAB*, and *MYL2*).

281

282 *Ethanol treatment alters multiple biological processes and molecular functions*

283 To determine the biological processes and molecular functions affected by ethanol treatment, we
284 performed GO analysis among the 198 down-regulated proteins in the ethanol-treated hiPSC-CM lysate
285 samples. This analysis resulted in 466 GO terms that were significantly enriched ($P < 0.05$). Of these terms,
286 283 terms belonged to biological process, 117 terms to cellular component, and 66 terms to molecular
287 function. To focus on more valuable GO terms, we excluded duplicate enriched GO terms, which had the
288 same corresponding protein lists, and filtered all the remaining GO terms with the following more stringent
289 criteria: $P < 0.01$, fold enrichment > 2 , and the number of involved proteins ≥ 5 . As shown in Fig. 3A, 159
290 GO terms met these criteria. The number of terms associated with biological process, cellular component
291 and molecular function was 97, 43 and 19, respectively. Specifically, as shown in Fig. 3A and Table 2,
292 ethanol exposure strikingly down-regulated the expression of proteins associated with the regulation of the
293 force of heart contraction (5 proteins), myofibril assembly (8 proteins), striated muscle cell development
294 (15 proteins), muscle system process (27 proteins), actin filament-based process (33 proteins), cytoskeleton
295 organization (46 proteins), sarcomere (24 proteins), and adherens junction (44 proteins).

296 In Fig. 3B, we present a detailed map showing the GO terms linked with specific differentially
297 expressed proteins that were associated with biological processes. In this analysis, individual proteins could
298 be linked with more than one GO terms. For example, integrin-linked kinase (ILK) is known to contribute
299 to wound healing, cell-cell adhesion, extracellular matrix organization, heart development, and myofibril;
300 caveolin 1 (CAV1) is involved in wound healing, response to transforming growth factor β (TGF- β),
301 response to oxygen-containing compound, cell-cell adhesion, and regulation of metal ion transport; actinin
302 alpha 2 (ACTN2) is involved in response to oxygen-containing compound, regulation of metal ion transport,
303 heart development, and myofibril; and filamin A (FLNA) is known to be involved in wound healing, cell-
304 cell adhesion, regulation of metal ion transport, and myofibril.

305 To further explore the potential underlying signaling pathways affected under ethanol treatment,
306 we performed KEGG pathway analysis on the 198 down-regulated proteins in the ethanol-treated cell lysate
307 samples. In this analysis, three of the top five significantly enriched pathways had connection to the GO
308 terms listed in Fig. 3B, including focal adhesion, ECM-receptor interaction, and regulation of actin
309 cytoskeleton (Fig. 4A). In addition, as a large number of differentially expressed proteins function as a part
310 of focal adhesion, we also delineated the protein-protein interaction among these proteins, which further
311 implicates their contributions to ethanol-induced cardiotoxicity in hiPSC-CMs (Fig. 4B). Notably, paxillin
312 (PXN), zyxin (ZYG), and actinin alpha 1 (ACTN1) interacted with multiple focal adhesion related proteins:
313 11 for PXN, 7 for ZYG and 6 for ACTN1.

314

315 DISCUSSION

316 Treatment with ethanol causes severe detrimental effects on hiPSC-CMs as indicated by significant
317 cell death and defective Ca^{2+} handling. By performing the proteomic and bioinformatic analysis, we have
318 identified proteins and pathways affected by ethanol treatment which aids in a better understanding of the
319 underlying molecular mechanisms.

320 Among the proteins that were significantly altered in ethanol-treated hiPSC-CMs, several are
321 known to contribute or respond to oxidative stress. This finding is consistent with our previous study

322 demonstrating that oxidative stress plays a central role in ethanol-induced cardiotoxicity at the cellular level
323 (Rampoldi et al., 2019). Specifically, glutathione peroxidase 1 (GPX1), a powerful ubiquitous enzyme that
324 can reduce cytosolic and mitochondrial reactive oxygen species (ROS), was 27% lower in ethanol-treated
325 hiPSC-CMs compared with untreated control which could disturb the balance between ROS and
326 antioxidants and result in oxidative stress (Espinosa-Diez et al., 2015). A second protein, poly(ADP-ribose)
327 polymerase-1 (PARP-1), was reduced by 24% following ethanol treatment. PARP-1 is the major isoform
328 of an expanding family of poly(ADP-ribosyl)ation enzymes which primarily functions as a DNA damage
329 sensor in the nucleus to modulate DNA repair and maintain genomic integrity (Virag and Szabo, 2002). It
330 is generally recognized that PARP-1 activation can exacerbate the deleterious pathophysiological effects in
331 CMs under oxidative stress, mainly through induction of mitochondrial dysfunction and promotion of
332 mitochondrial cell death pathways (Chen et al., 2004). A third protein, voltage-dependent anion-selective
333 channel protein (VDAC), was reduced by 48% under ethanol treatment. VDAC1 is the most abundant
334 isoform in the heart (Tian et al., 2019) and functions as a positive regulator of mitochondria-mediated
335 apoptosis since it is a target for the pro-apoptotic protein BAX and is involved in the release of apoptotic
336 proteins located in the intermembrane space of mitochondria (Li et al., 2016). Another protein, Corin (a
337 transmembrane serine protease identified in the heart), was increased by 35% in hiPSC-CMs treated with
338 ethanol. Increased expression of Corin in hiPSC-CMs probably reflects its potential role in counter-acting
339 ethanol cardiotoxicity because Corin is reported to protect CMs under oxidative stress via diminishing
340 apoptosis (Sullivan et al., 2020).

341 Stress-related proteins that we found to be dysregulated in ethanol-treated hiPSC-CMs also include
342 four small heat shock proteins (sHSPs). The human family of sHSPs (also refers to HSPBs) is constituted
343 by 10 proteins (HSPB1-10), which has been shown to be crucial in maintaining the function and integrity
344 of a wide range of cell types and tissues under stress conditions (Kampinga and Garrido, 2012). Specifically,
345 by their expression level, HSPB6 (also refers to HSP20) was decreased by 44%, HSPB2 was decreased by
346 31%, HSPB5 (also refers to CRYAB) was decreased by 58%, and HSPB1 (also refers to HSP27) was
347 increased by 39%. These four HSPBs are all recognized to have cardio-protective effects in the heart against

348 stress-induced injuries including MI and cardiac hypertrophy, mainly through modulating apoptotic process
349 (Wang et al., 2019; Mitra et al., 2013). Particularly, studies have shown that HSPB1 is an essential regulator
350 on alleviating inflammation in myocardial repair after MI and maintaining cardiac function against atrial
351 fibrillation (Wang et al., 2019; Brundel et al., 2006). Taken all together, ethanol can suppress as well as
352 evoke the defense system against oxidative stress related apoptosis in hiPSC-CMs. These proteins could be
353 promising targets to reduce ethanol-induced cardiotoxicity.

354 Alteration in the expression of ion channel related proteins represents another category of the
355 differentially expressed proteins in hiPSC-CMs treated with ethanol. This finding is consistent with the
356 observation that treatment of hiPSC-CMs with ethanol triggered Ca^{2+} transient abnormality as well as the
357 growing evidence that ethanol exposure increases the risk of arrhythmias and negative inotropic effects via
358 Ca^{2+} handling defects and disordered excitation-contraction coupling (Voskoboinik et al., 2016; Mustroph
359 et al., 2019; Mustroph et al., 2018). Since the ion transporting requires the assistance of certain ion channels
360 and exchangers, the down-regulation of several proteins related to regulation of metal ion channels in
361 ethanol-treated hiPSC-CMs could be partially responsible for the CM dysfunction. For example, annexin 6
362 (ANXA6) is one of the abundant annexins in myocardium which has been shown to regulate Ca^{2+} influx
363 via modulating the activity of the L-type Ca^{2+} channel and to regulate Ca^{2+} release via modulating the
364 activity of the ryanodine receptor 2 (RyR2) and Na^+/Ca^{2+} exchanger (Matteo and Moravec, 2000). ATPase
365 Na^+/K^+ transporting subunit $\alpha 2$ (ATP1A2) composes a part of the Na^+/K^+ pump which can move Na^+ from
366 the cytoplasm to the extracellular space in order to maintain Na^+ homeostasis (Shattock et al., 2015). Studies
367 have also shown that ATP1A2 can regulate intracellular Ca^{2+} signaling, contractility and pathological
368 hypertrophy (Liu et al., 2016). In this work, we found that the ANXA6 level was decreased by 40% and
369 that ATP1A2 level was decreased by 29%.

370 Other differentially expressed proteins in ethanol-treated hiPSC-CMs that could affect contractility
371 of the cells include some myofibril structure proteins. These myofibril structure proteins were significantly
372 down-regulated in hiPSC-CMs exposed to ethanol: myosin light chain 2/3 (MYL2/3), Sorbin and SH3
373 domain-containing protein 2 (SORBS2), myozenin 2 (MYOZ2), cysteine and glycine rich protein 3

374 (CSRP3), and ACTN1/2. Dysregulation of any of these proteins can impact cardiac contraction or even
375 lead to the development of dilated or hypertrophic cardiomyopathy and heart failure (Pauly, 2011; Li et al.,
376 2019; Bang, 2017; Frey et al., 2004; Wang et al., 2016; Chiu et al., 2010). Hence, the alteration in the
377 expression of ion channels and contractile fiber structure-related proteins could be connected to the
378 corresponding molecular mechanisms of the occurrence of arrhythmias and dysfunctional contraction
379 induced by ethanol.

380 Our proteomic analysis also reveals the down-regulation of focal adhesion proteins in hiPSC-CMs
381 treated with ethanol. Focal adhesions are complexes of a variety of transmembrane, cytoplasmic proteins,
382 and enzymes that link ECM to the cytoskeleton (Swaminathan et al., 2017). Focal adhesions mediate
383 signaling from ECM to different cellular responses, including proliferation and cell (Vitulo et al., 2016).
384 Considering the role of focal adhesion proteins in cell death, their decreased abundances can imply possible
385 role of focal adhesion proteins in ethanol-induced cardiotoxicity. Among those focal adhesion proteins
386 affected by ethanol treatment, ILK is a multifunctional protein that regulates cell–matrix–cytoskeletal
387 interactions and plays a critical role in ECM-mediated signaling pathway, contributing to various cellular
388 phenomena including growth, repair, and contractility (Hannigan et al., 2007). ILK is reported to modulate
389 the spontaneous beating rate and Ca^{2+} uptake in hiPSC-CMs—it can mediate CM force transduction
390 through regulation of the Ca^{2+} regulatory protein sarco/endoplasmic reticulum Ca^{2+} -ATPase (SERCA)
391 (Traister et al., 2014). In addition, ILK has cardio-protective property on CMs during dilated
392 cardiomyopathy and heart failure (White et al., 2006), whereas inhibition of ILK induces cell apoptosis
393 (McDonald et al., 2008). In line with the findings of increased cell death, defective Ca^{2+} handling, and
394 decreased contractility in ethanol-treated hiPSC-CMs, ILK could serve as a pivotal upstream regulator in
395 all of these toxic events.

396 Several other focal adhesion proteins were down-regulated by ethanol treatment of hiPSC-CMs.
397 PXN is a focal adhesion-associated adaptor protein that recruits diverse signaling proteins to focal
398 adhesions to guarantee regular signal reception and transduction (Schaller, 2001). It is responsible to
399 modulate the expression of stretch-responsive genes via interacting with ILK, Parvin, and PINCH, the

400 deficiency of which can lead to contractile disability and even heart failure (Hirth et al., 2016). Herein, the
401 expression levels of PXN and Parvin β (PARVB) were decreased in ethanol-treated hiPSC-CMs, which
402 could be one of the reasons for ethanol-induced contractility reduction. In addition, the other down-
403 regulated proteins, ZYX, FLNA, talin 2 (TLN2), and ACTN1/2, are crucial to intracellular contractile force
404 transduction (Santoro et al., 2019). Furthermore, CAV1 is a versatile focal adhesion protein that is also
405 known to regulate TGF- β signaling pathway, Ca²⁺ signaling, and oxidative stress (Shihata et al., 2017). The
406 decreased level of CAV1 in hiPSC-CMs exposed to ethanol could therefore play multiple roles in TGF- β -
407 mediated apoptosis and fibrosis and increased risk of arrhythmias. Together, dysregulation of focal
408 adhesion proteins could be a prominent mechanism underlying ethanol-induced cardiotoxicity.

409 In addition, among the differentially expressed proteins identified in this study, some were also
410 found to be differentially expressed at the RNA level. Intriguingly, 4 were involved in focal adhesion (*FHL1*,
411 *MCAM*, *AJUBA*, and *ZYX*) and 4 were relevant to myofibril (*CSR3*, *MYOZ2*, *CRYAB*, and *MYL2*). These
412 findings suggest the important role that focal adhesion and myofibril related proteins play in ethanol-
413 induced cardiotoxicity.

414 Finally, the current results also reveal potential involvement of other signaling pathways in ethanol-
415 induced cardiotoxicity. For example, two proteins associated with the TRAF2 signaling were significantly
416 down-regulated by ethanol treatment. One of them, CPNE1, is a Ca²⁺-dependent lipid-binding protein and
417 CPNE1 overexpression upregulates TRAF2 expression (Liang et al., 2017). The other one, TNIK, is a
418 TRAF2 and NCK interacting kinase and functions as an activator of the Wnt signaling pathway.

419 A limitation of this study is that our bioinformatics analyses were performed in a human
420 cardiomyocyte cell model. Consequently, physiological translation of our findings in either rodent or human
421 tissues remains to be established. Nevertheless, given that hiPSC-CMs are physiologically relevant to
422 human CMs, our findings provide interesting leads for further studies in vivo.

423 In conclusion, we have systemically and quantitatively investigated the expression changes of
424 proteins in the lysates and media of hiPSC-CMs following the treatment with ethanol. Consistent with the
425 cell-level assessments including decreased cell survival and impaired CM function, many dysregulated

426 proteins have been found to be involved in wound healing, apoptosis, oxidative stress, heart contraction,
427 and regulation of metal ion transport. Expression of focal adhesion and ECM related proteins is also down-
428 regulated, including ILK, PXN, and CAV1. Furthermore, the current study reveals a novel role for proteins
429 associated with the TRAF2 signaling in cardiotoxicity induced by ethanol treatment.

430

431 SUPPORTING INFORMATION

432 Fig. S1. Schematic diagrams of the experimental design

433 Table S1. Information of major reagents

434 Table S2. Antibodies for immunocytochemistry

435

436 FUNDING

437 This study was supported by the National Institutes of Health [R21AA025723 and R01HL136345]; NSF-
438 CASIS (National Science Foundation-Center for the Advancement of Science in Space) [CBET 1926387];
439 the Center for Pediatric Technology at Emory University; and Georgia Institute of Technology; and
440 Imagine, Innovate and Impact (I3) Funds from the Emory School of Medicine and through the Georgia
441 CTSA NIH award [UL1-TR002378].

442

443 CONFLICT OF INTEREST

444 The authors declare no competing financial interests.

445

446 AUTHOR CONTRIBUTIONS

447 R.L., F.S., R.W., and C.X. designed experiments. R.L., F.S., A.R., and D.L. performed experiments. R.L.,
448 F.S., P.F., and L.C.A. analyzed data. R.L., F.S., P.F., R.W., and C.X. wrote the manuscript. All authors
449 contributed to the discussion of results and editing and final approval of the manuscript.

450

451 REFERENCES

- 452 Aebersold R, Mann M (2016) Mass-spectrometric exploration of proteome structure and function. *Nature*
453 537: 347-55.
- 454 Bang ML (2017) Animal models of congenital cardiomyopathies associated with mutations in Z-Line
455 proteins. *J Cell Physiol* 232: 38-52.
- 456 Brandt M, Garlapati V, Oelze M, Sotiriou E, Knorr M, Kroller-Schon S, Kossmann S, Schonfelder T,
457 Morawietz H, Schulz E, Schultheiss HP, Daiber A, Munzel T, Wenzel P (2016) NOX2 amplifies
458 acetaldehyde-mediated cardiomyocyte mitochondrial dysfunction in alcoholic cardiomyopathy. *Sci*
459 *Rep* 6: 32554.
- 460 Brundel BJ, Shiroshita-Takeshita A, Qi X, Yeh YH, Chartier D, van Gelder IC, Henning RH, Kampinga
461 HH, Nattel S (2006) Induction of heat shock response protects the heart against atrial fibrillation.
462 *Circ Res* 99: 1394-402.
- 463 Burridge PW, Matsa E, Shukla P, Lin ZC, Churko JM, Ebert AD, Lan F, Diecke S, Huber B, Mordwinkin
464 NM, Plews JR, Abilez OJ, Cui B, Gold JD, Wu JC (2014) Chemically defined generation of human
465 cardiomyocytes. *Nat Methods* 11: 855-60.
- 466 Chen M, Zsengeller Z, Xiao CY, Szabo C (2004) Mitochondrial-to-nuclear translocation of apoptosis-
467 inducing factor in cardiac myocytes during oxidant stress: potential role of poly(ADP-ribose)
468 polymerase-1. *Cardiovasc Res* 63: 682-8.
- 469 Chiu C, Bagnall RD, Ingles J, Yeates L, Kennerson M, Donald JA, Jormakka M, Lind JM, Semsarian C
470 (2010) Mutations in alpha-actinin-2 cause hypertrophic cardiomyopathy: a genome-wide analysis.
471 *J Am Coll Cardiol* 55: 1127-35.
- 472 Day E, Rudd JHF (2019) Alcohol use disorders and the heart. *Addiction* 114: 1670-1678.
- 473 Elias JE, Gygi SP (2007) Target-decoy search strategy for increased confidence in large-scale protein
474 identifications by mass spectrometry. *Nat Methods* 4: 207-14.

475 Eng JK, McCormack AL, Yates JR (1994) An approach to correlate tandem mass spectral data of peptides
476 with amino acid sequences in a protein database. *Journal of The American Society for Mass*
477 *Spectrometry* 5: 976-89.

478 Espinosa-Diez C, Miguel V, Mennerich D, Kietzmann T, Sanchez-Perez P, Cadenas S, Lamas S (2015)
479 Antioxidant responses and cellular adjustments to oxidative stress. *Redox Biol* 6: 183-197.

480 Frey N, Barrientos T, Shelton JM, Frank D, Rutten H, Gehring D, Kuhn C, Lutz M, Rothermel B, Bassel-
481 DUBY R, Richardson JA, Katus HA, Hill JA, Olson EN (2004) Mice lacking calstabin-1 are
482 sensitized to calcineurin signaling and show accelerated cardiomyopathy in response to
483 pathological biomechanical stress. *Nat Med* 10: 1336-43.

484 GBD 2016 Alcohol Collaborators (2018) Alcohol use and burden for 195 countries and territories, 1990-
485 2016: a systematic analysis for the Global Burden of Disease Study 2016. *Lancet* 392: 1015-1035.

486 Guo R, Hu N, Kandadi MR, Ren J (2012) Facilitated ethanol metabolism promotes cardiomyocyte
487 contractile dysfunction through autophagy in murine hearts. *Autophagy* 8: 593-608.

488 Hannigan GE, Coles JG, Dedhar S (2007) Integrin-linked kinase at the heart of cardiac contractility, repair,
489 and disease. *Circ Res* 100: 1408-14.

490 Hirth S, Buhler A, Buhrdel JB, Rudeck S, Dahme T, Rottbauer W, Just S (2016) Paxillin and focal adhesion
491 kinase (FAK) regulate cardiac contractility in the zebrafish heart. *PLoS One* 11: e0150323.

492 Huang DW, Sherman BT, Lempicki RA (2008) Systematic and integrative analysis of large gene lists using
493 DAVID bioinformatics resources. *Nature Protocols* 4: 44.

494 Isserlin R, Merico D, Alikhani-Koupaei R, Gramolini A, Bader GD, Emili A (2010) Pathway analysis of
495 dilated cardiomyopathy using global proteomic profiling and enrichment maps. *Proteomics* 10:
496 1316-27.

497 Jha R, Wu Q, Singh M, Preininger MK, Han P, Ding G, Cho HC, Jo H, Maher KO, Wagner MB, Xu C
498 (2016) Simulated microgravity and 3D culture enhance induction, viability, proliferation and
499 differentiation of cardiac progenitors from human pluripotent stem cells. *Sci Rep* 6: 30956.

500 Kall L, Canterbury JD, Weston J, Noble WS, MacCoss MJ (2007) Semi-supervised learning for peptide
501 identification from shotgun proteomics datasets. *Nat Methods* 4: 923-5.

502 Kampinga HH, Garrido C (2012) HSPBs: small proteins with big implications in human disease. *Int J*
503 *Biochem Cell Biol* 44: 1706-10.

504 Li X, Lu WJ, Li Y, Wu F, Bai R, Ma S, Dong T, Zhang H, Lee AS, Wang Y, Lan F (2019) MLP-deficient
505 human pluripotent stem cell derived cardiomyocytes develop hypertrophic cardiomyopathy and
506 heart failure phenotypes due to abnormal calcium handling. *Cell Death Dis* 10: 610.

507 Li X, Wang H, Yao B, Xu W, Chen J, Zhou X (2016) lncRNA H19/miR-675 axis regulates cardiomyocyte
508 apoptosis by targeting VDAC1 in diabetic cardiomyopathy. *Sci Rep* 6: 36340.

509 Liang J, Zhang J, Ruan J, Mi Y, Hu Q, Wang Z, Wei B (2017) CPNE1 is a useful prognostic marker and is
510 associated with TNF receptor-associated factor 2 (TRAF2) expression in prostate cancer. *Med Sci*
511 *Monit* 23: 5504-5514.

512 Liu L, Wu J, Kennedy DJ (2016) Regulation of cardiac remodeling by cardiac Na⁽⁺⁾/K⁽⁺⁾-ATPase isoforms.
513 *Front Physiol* 7: 382.

514 Maiuolo J, Maretta A, Gliozzi M, Musolino V, Carresi C, Bosco F, Mollace R, Scarano F, Palma E,
515 Scicchitano M, Nucera S, Sergi D, Muscoli S, Gratteri S, Muscoli C, Mollace V (2018) Ethanol-
516 induced cardiomyocyte toxicity implicit autophagy and NF-κB transcription factor. *Pharmacol Res*
517 133: 141-150.

518 Mann M (2016) Origins of mass spectrometry-based proteomics. *Nat Rev Mol Cell Biol* 17: 678.

519 Matteo RG, Moravec CS (2000) Immunolocalization of annexins IV, V and VI in the failing and non-failing
520 human heart. *Cardiovasc Res* 45: 961-70.

521 McDonald PC, Fielding AB, Dedhar S (2008) Integrin-linked kinase--essential roles in physiology and
522 cancer biology. *J Cell Sci* 121: 3121-32.

523 Mitra A, Basak T, Datta K, Naskar S, Sengupta S, Sarkar S (2013) Role of alpha-crystallin B as a regulatory
524 switch in modulating cardiomyocyte apoptosis by mitochondria or endoplasmic reticulum during
525 cardiac hypertrophy and myocardial infarction. *Cell Death Dis* 4: e582.

526 Mustroph J, Lebek S, Maier LS, Neef S (2019) Mechanisms of cardiac ethanol toxicity and novel treatment
527 options. *Pharmacol Ther* 197: 1-10.

528 Mustroph J, Wagemann O, Lebek S, Tarnowski D, Ackermann J, Drzymalski M, Pabel S, Schmid C,
529 Wagner S, Sossalla S, Maier LS, Neef S (2018) SR Ca(2+)-leak and disordered excitation-
530 contraction coupling as the basis for arrhythmogenic and negative inotropic effects of acute ethanol
531 exposure. *J Mol Cell Cardiol* 116: 81-90.

532 Orlando E, Aebersold R (2019) On the contribution of mass spectrometry-based platforms to the field of
533 personalized oncology. *Trends in Analytical Chemistry* 110: 129-142.

534 Pauly DF (2011) The slow cardiac myosin regulatory light chain in heart failure. *Clin Cardiol* 34: 10-1.

535 Peng Y, Gregorich ZR, Valeja SG, Zhang H, Cai W, Chen YC, Guner H, Chen AJ, Schwahn DJ, Hacker
536 TA, Liu X, Ge Y (2014) Top-down proteomics reveals concerted reductions in myofilament and
537 Z-disc protein phosphorylation after acute myocardial infarction. *Mol Cell Proteomics* 13: 2752-
538 64.

539 Pinheiro EA, Fetterman KA, Burridge PW (2019) hiPSCs in cardio-oncology: deciphering the genomics.
540 *Cardiovasc Res* 115: 935-948.

541 Rampoldi A, Singh M, Wu Q, Duan M, Jha R, Maxwell JT, Bradner JM, Zhang X, Saraf A, Miller GW,
542 Gibson G, Brown LA, Xu C (2019) Cardiac toxicity from ethanol exposure in human-induced
543 pluripotent stem cell-derived cardiomyocytes. *Toxicol Sci* 169: 280-292.

544 Roozen S, Peters GJ, Kok G, Townend D, Nijhuis J, Curfs L (2016) Worldwide prevalence of fetal alcohol
545 spectrum disorders: a systematic literature review including meta-analysis. *Alcohol Clin Exp Res*
546 40: 18-32.

547 Santoro R, Perrucci GL, Gowran A, Pompilio G (2019) Unchain my heart: integrins at the basis of iPSC
548 cardiomyocyte differentiation. *Stem Cells Int* 2019: 8203950.

549 Schaller MD (2001) Paxillin: a focal adhesion-associated adaptor protein. *Oncogene* 20: 6459-72.

550 Shannon P, Markiel A, Ozier O, Baliga NS, Wang JT, Ramage D, Amin N, Schwikowski B, Ideker T (2003)
551 Cytoscape: a software environment for integrated models of biomolecular interaction networks.
552 Genome Research 13: 2498-2504.

553 Shattock MJ, Ottolia M, Bers DM, Blaustein MP, Boguslavskyi A, Bossuyt J, Bridge JH, Chen-Izu Y,
554 Clancy CE, Edwards A, Goldhaber J, Kaplan J, Lingrel JB, Pavlovic D, Philipson K, Sipido KR,
555 Xie ZJ (2015) Na⁺/Ca²⁺ exchange and Na⁺/K⁺-ATPase in the heart. J Physiol 593: 1361-82.

556 Shihata WA, Putra MRA, Chin-Dusting JPF (2017) Is there a potential therapeutic role for caveolin-1 in
557 fibrosis? Front Pharmacol 8: 567.

558 Sullivan RD, Houg AK, Gladysheva IP, Fan TM, Tripathi R, Reed GL, Wang D (2020) Corin
559 overexpression reduces myocardial infarct size and modulates cardiomyocyte apoptotic cell death.
560 Int J Mol Sci 21.

561 Swaminathan V, Kalappurakkal JM, Mehta SB, Nordenfelt P, Moore TI, Koga N, Baker DA, Oldenbourg
562 R, Tani T, Mayor S, Springer TA, Waterman CM (2017) Actin retrograde flow actively aligns and
563 orients ligand-engaged integrins in focal adhesions. Proc Natl Acad Sci U S A 114: 10648-10653.

564 Szklarczyk D, Franceschini A, Wyder S, Forslund K, Heller D, Huerta-Cepas J, Simonovic M, Roth A,
565 Santos A, Tsafou KP, Kuhn M, Bork P, Jensen LJ, von Mering C (2014) STRING v10: protein–
566 protein interaction networks, integrated over the tree of life. Nucleic Acids Research 43: D447-
567 D452.

568 Tan Y, Li X, Prabhu SD, Brittan KR, Chen Q, Yin X, McClain CJ, Zhou Z, Cai L (2012) Angiotensin II
569 plays a critical role in alcohol-induced cardiac nitrative damage, cell death, remodeling, and
570 cardiomyopathy in a protein kinase C/nicotinamide adenine dinucleotide phosphate oxidase-
571 dependent manner. J Am Coll Cardiol 59: 1477-86.

572 Tian M, Xie Y, Meng Y, Ma W, Tong Z, Yang X, Lai S, Zhou Y, He M, Liao Z (2019) Resveratrol protects
573 cardiomyocytes against anoxia/reoxygenation via dephosphorylation of VDAC1 by Akt-GSK3
574 beta pathway. Eur J Pharmacol 843: 80-87.

575 Tomlinson L, Lu ZQ, Bentley RA, Colley HE, Murdoch C, Webb SD, Cross MJ, Copples IM, Sharma P
576 (2019) Attenuation of doxorubicin-induced cardiotoxicity in a human in vitro cardiac model by the
577 induction of the NRF-2 pathway. *Biomed Pharmacother* 112: 108637.

578 Traister A, Li M, Aafaqi S, Lu M, Arab S, Radisic M, Gross G, Guido F, Sherret J, Verma S, Slorach C,
579 Mertens L, Hui W, Roy A, Delgado-Olguin P, Hannigan G, Maynes JT, Coles JG (2014) Integrin-
580 linked kinase mediates force transduction in cardiomyocytes by modulating SERCA2a/PLN
581 function. *Nat Commun* 5: 4533.

582 Tyanova S, Temu T, Sinitcyn P, Carlson A, Hein MY, Geiger T, Mann M, Cox J (2016) The Perseus
583 computational platform for comprehensive analysis of proteomics data. *Nature Methods* 13: 731-
584 740.

585 Virag L, Szabo C (2002) The therapeutic potential of poly(ADP-ribose) polymerase inhibitors. *Pharmacol*
586 *Rev* 54: 375-429.

587 Vitillo L, Baxter M, Iskender B, Whiting P, Kimber SJ (2016) Integrin-associated focal adhesion kinase
588 protects human embryonic stem cells from apoptosis, detachment, and differentiation. *Stem Cell*
589 *Reports* 7: 167-76.

590 Voskoboinik A, Prabhu S, Ling LH, Kalman JM, Kistler PM (2016) Alcohol and atrial fibrillation: a
591 sobering review. *J Am Coll Cardiol* 68: 2567-2576.

592 Wang H, Bei Y, Shen S, Huang P, Shi J, Zhang J, Sun Q, Chen Y, Yang Y, Xu T, Kong X, Xiao J (2016)
593 miR-21-3p controls sepsis-associated cardiac dysfunction via regulating SORBS2. *J Mol Cell*
594 *Cardiol* 94: 43-53.

595 Wang Y, Liu J, Kong Q, Cheng H, Tu F, Yu P, Liu Y, Zhang X, Li C, Li Y, Min X, Du S, Ding Z, Liu L
596 (2019) Cardiomyocyte-specific deficiency of HSPB1 worsens cardiac dysfunction by activating
597 NFkappaB-mediated leucocyte recruitment after myocardial infarction. *Cardiovasc Res* 115: 154-
598 167.

599 White AM, Castle IP, Hingson RW, Powell PA (2020) Using death certificates to explore changes in
600 alcohol-related mortality in the United States, 1999 to 2017. *Alcohol Clin Exp Res* 44: 178-187.

601 White DE, Coutu P, Shi YF, Tardif JC, Nattel S, St Arnaud R, Dedhar S, Muller WJ (2006) Targeted
602 ablation of ILK from the murine heart results in dilated cardiomyopathy and spontaneous heart
603 failure. *Genes Dev* 20: 2355-60.

604 Whitman IR, Agarwal V, Nah G, Dukes JW, Vittinghoff E, Dewland TA, Marcus GM (2017) Alcohol
605 abuse and cardiac disease. *J Am Coll Cardiol* 69: 13-24.

606 Xiao H, Chen W, Tang GX, Smeeckens JM, Wu R (2015) Systematic investigation of cellular response and
607 pleiotropic effects in atorvastatin-treated liver cells by MS-based proteomics. *J Proteome Res* 14:
608 1600-11.

609 Zhang S, Wang L, Yang T, Chen L, Zhao L, Wang T, Chen L, Ye Z, Zheng Z, Qin J (2020) Parental alcohol
610 consumption and the risk of congenital heart diseases in offspring: An updated systematic review
611 and meta-analysis. *Eur J Prev Cardiol* 27: 410-421.

612

613 **Table 1.** Top up-regulated and down-regulated proteins in hiPSC-CMs treated with ethanol compared with
614 no treatment

Regulation	Symbol	Description	Fold Change	<i>P</i> -value
Up	BST2	Bone marrow stromal cell antigen 2	1.42	0.0030
	CORIN	Corin, serine peptidase	1.35	0.0332
	VTN	Vitronectin	1.30	0.0212
Down	DMXL2	DmX-like protein 2	0.33	0.0103
	CRYAB	Alpha-crystallin B chain	0.42	0.0007
	H1-3	Histone H1.3	0.48	0.0027
	H1-2	Histone H1.2	0.50	0.0040
	FN3KRP	Ketosamine-3-kinase	0.53	0.0118
	H1-0	Histone H1.0	0.53	0.0069
	HSPB6	Heat shock protein beta-6	0.56	0.0015
	SORBS2	Sorbin and SH3 domain-containing protein 2	0.56	0.0094
	MYL2	Myosin regulatory light chain 2	0.56	0.0027
	ANXA3	Annexin A3	0.57	0.0121
	CPNE1	Copine-1	0.58	0.0295
	CD59	CD59 glycoprotein	0.58	0.0227
	SLMAP	Sarcolemmal membrane-associated protein	0.58	0.0371
	NEXN	Nexilin	0.60	0.0110
	ANXA6	Annexin A6	0.60	0.0464
	FLNA	Filamin-A	0.60	0.0133
	CAVIN4	Caveolae-associated protein 4	0.60	0.0076
XIRP1	Xin actin-binding repeat-containing protein 1	0.60	0.0086	
AKAP2	A-kinase anchor protein 2	0.60	0.0262	

H1-4	Histone H1.4	0.60	0.0109
AJUBA	LIM domain-containing protein ajuba	0.60	0.0238
OR1D4	Olfactory receptor 1D4	0.60	0.0415
LMO7	LIM domain only protein 7	0.60	0.0252
DNAJC6	Putative tyrosine-protein phosphatase auxilin	0.61	0.0025
SH3KBP1	SH3 domain-containing kinase-binding protein 1	0.61	0.0124
FHL1	Four and a half LIM domains protein 1	0.61	0.0100
FERMT2	Fermitin family homolog 2	0.61	0.0443

615

616

617 **Table 2.** Top down-regulated GO terms in hiPSC-CMs treated with ethanol compared with no treatment

ID	GO Term Description	Count	Fold Enrichment	P-value
GO:0005912	Adherens junction	44	6.53	4.41E-23
GO:0070161	Anchoring junction	44	6.37	1.13E-22
GO:0030054	Cell junction	56	4.18	1.57E-20
GO:0008092	Cytoskeletal protein binding	46	5.04	1.08E-19
GO:0030017	Sarcomere	24	13.14	4.80E-19
GO:0030016	Myofibril	25	12.14	4.94E-19
GO:0043228	Non-membrane-bounded organelle	93	2.38	1.12E-18
GO:0043232	Intracellular non-membrane-bounded organelle	93	2.38	1.12E-18
GO:0031674	I band	21	16.51	1.24E-18
GO:0015629	Actin cytoskeleton	33	7.28	1.70E-18
GO:0043292	Contractile fiber	25	11.49	1.80E-18
GO:0003779	Actin binding	32	7.48	2.85E-18
GO:0044449	Contractile fiber part	24	12.05	3.43E-18
GO:0005856	Cytoskeleton	64	3.21	6.86E-18
GO:0005925	Focal adhesion	30	7.90	9.69E-18
GO:0005924	Cell-substrate adherens junction	30	7.84	1.19E-17
GO:0030055	Cell-substrate junction	30	7.74	1.67E-17
GO:0030018	Z disc	18	15.71	1.55E-15
GO:0007010	Cytoskeleton organization	46	3.75	8.83E-15
GO:0005737	Cytoplasm	151	1.44	4.12E-14
GO:0003012	Muscle system process	27	6.22	1.85E-13
GO:0030029	Actin filament-based process	33	4.58	8.67E-13

GO:0005829	Cytosol	74	2.24	1.64E-12
GO:0005911	Cell-cell junction	30	4.80	4.18E-12
GO:0044822	Poly(A) RNA binding	43	3.33	4.61E-12
GO:0005515	Protein binding	158	1.36	4.66E-12
GO:0030036	Actin cytoskeleton organization	29	4.89	6.50E-12
GO:0005913	Cell-cell adherens junction	22	6.82	9.88E-12
GO:0050839	Cell adhesion molecule binding	26	5.23	2.6E-11
GO:0005198	Structural molecule activity	33	3.91	5.52E-11

618

619

FIGURE LEGENDS

620

621

622 **Fig. 1.** Ethanol treatment induces the death of hiPSC-CMs and defect in Ca²⁺ handling. (A) Representative
623 images of immunocytochemistry showing the majority of the cells in culture were positive for cardiac
624 markers at day 17. (B) Normalized cell viability in hiPSC-CMs exposed to 0 and 100 mM of ethanol for 5
625 days (n = 4). (C) Representative traces showing intracellular Ca²⁺ transients in hiPSC-CMs. Type i: normal
626 Ca²⁺ transients; Types ii to vi: abnormal Ca²⁺ transients. (D) Proportions of hiPSC-CMs exhibiting normal
627 (blue) and abnormal Ca²⁺ transients (red) following the treatment with 0 and 100 mM of ethanol for 5 days
628 are shown with the larger pie graphs. The distribution of the abnormal Ca²⁺ transient subtypes are shown
629 with the smaller pie graphs. The number of cells analyzed were 85 for 100 mM and 24 for untreated. ***,
630 *P*-value < 0.001; ****, *P*-value < 0.0001.

631

632 **Fig. 2.** Quantitative analysis of the proteome and secretome of hiPSC-CMs treated with ethanol. (A) The
633 workflow to characterize the alteration of protein expression in cell lysates and media caused by ethanol
634 exposure. (B) Reproducibility of the biological triplicates from each cell lysate sample. The number
635 represents Pearson's correlation coefficient (r). (C) Volcano plots illustrating proteins in cell lysates and
636 media with statistically significant difference in their abundance in ethanol-treated vs. untreated hiPSC-
637 CMs. (D) Heatmap presenting the overlapped DEGs identified by both of proteomics and RNA-Seq
638 analyses of the cell lysates. The squares of red and blue colors represented the log₂(fold change). FC, fold
639 change.

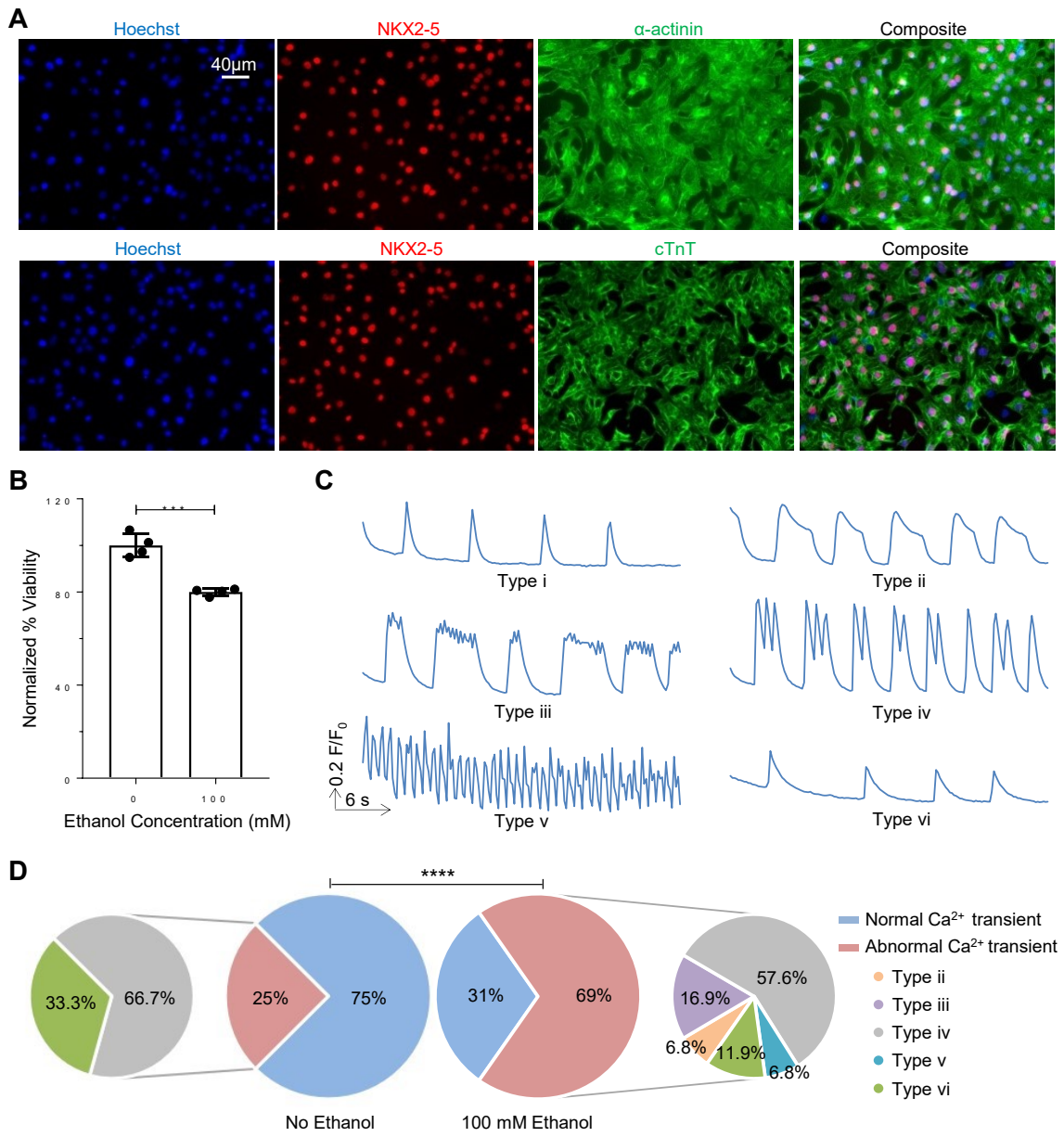
640

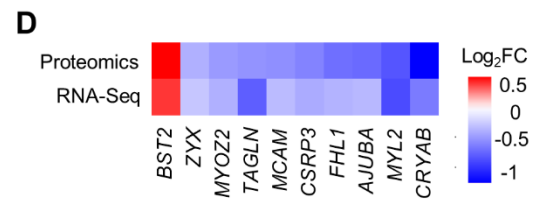
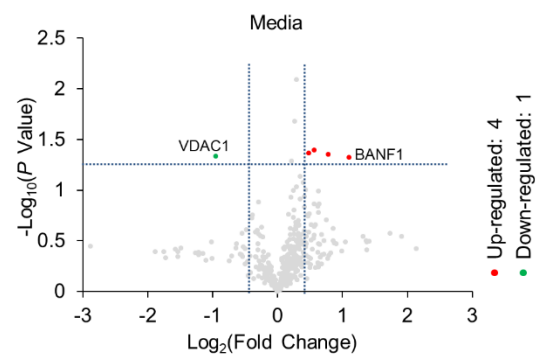
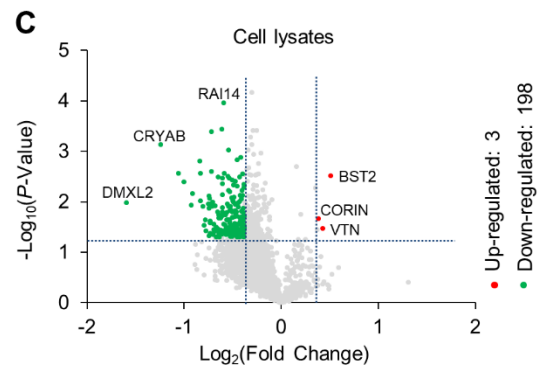
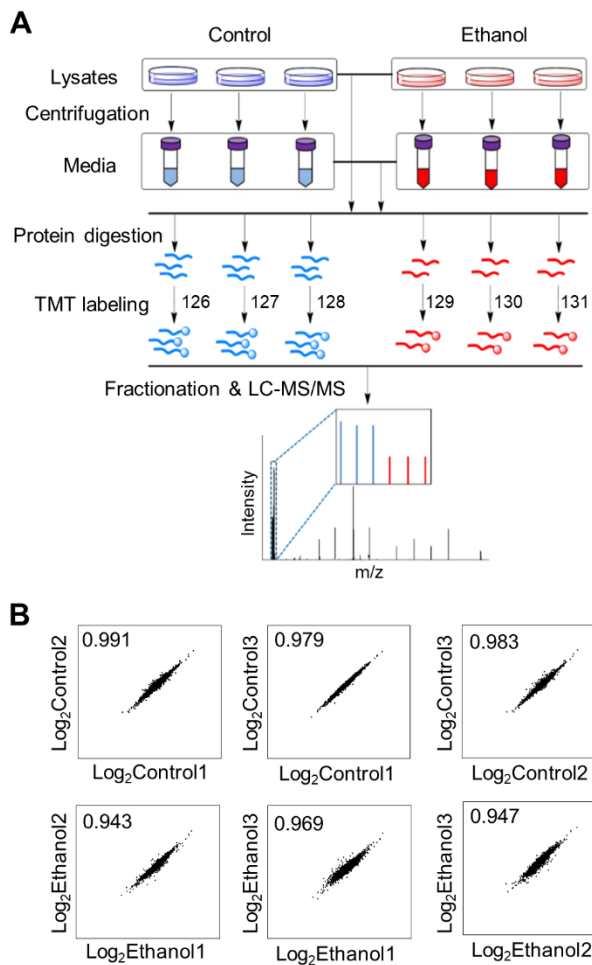
641 **Fig. 3.** GO enrichment analysis of the down-regulated proteins in ethanol-treated vs. untreated cell lysates
642 identified by MS-based proteomics. (A) Bubble plot showing GO terms with *P*-value < 0.01, fold
643 enrichment > 2, and protein count ≥ 5. The area of bubbles indicates the number of involved proteins in
644 each GO term. BP, biological process; CC, cellular component; MF, molecular function. (B) Chord diagram

645 showing connections between the down-regulated proteins and interested GO terms of biological process.
646 GO terms were presented on the right, and proteins contributing to these enrichments were drawn on the
647 left. The $\log_2(\text{fold change})$ for each gene is indicated with the color (yellow, green, and purple) in the
648 rectangles next to the gene name, and the key to the color is provided near the bottom of the chord diagram.

649
650 **Fig. 4.** KEGG enrichment and protein network analyses of the down-regulated proteins in ethanol-treated
651 vs. untreated cell lysates identified in the proteomics experiment. (A) Chord plot showing the down-
652 regulated proteins and associated KEGG clusters. KEGG pathways were presented on the right, and
653 proteins contributing to these enrichments were drawn on the left. (B) Interaction network of down-
654 regulated proteins involved in focal adhesion. The $\log_2(\text{fold change})$ for each gene is indicated with the
655 color (yellow, green, and purple) in the oval surrounding the gene name, and the key to the color is provided.
656 The protein list of focal adhesion was the same as in the KEGG pathway except 2 proteins that did not show
657 any interaction at the interaction score above 0.7.

658

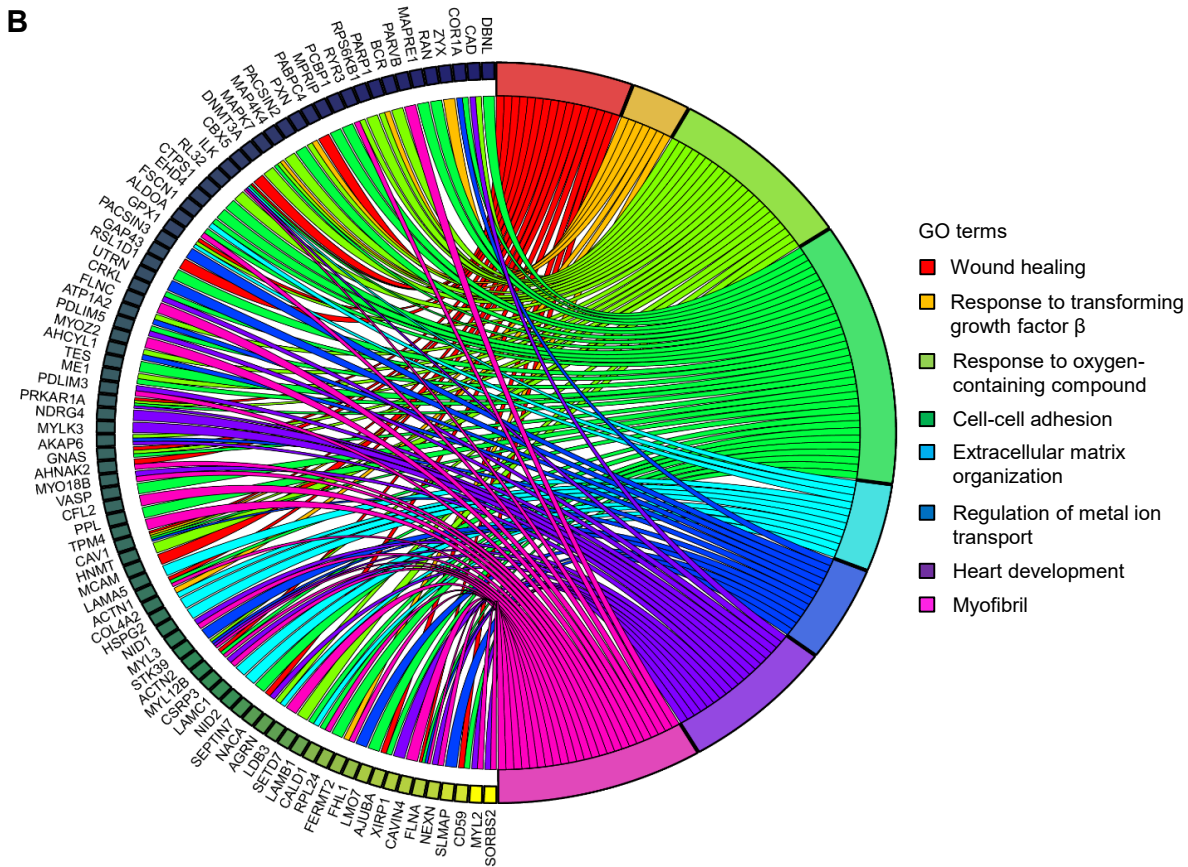
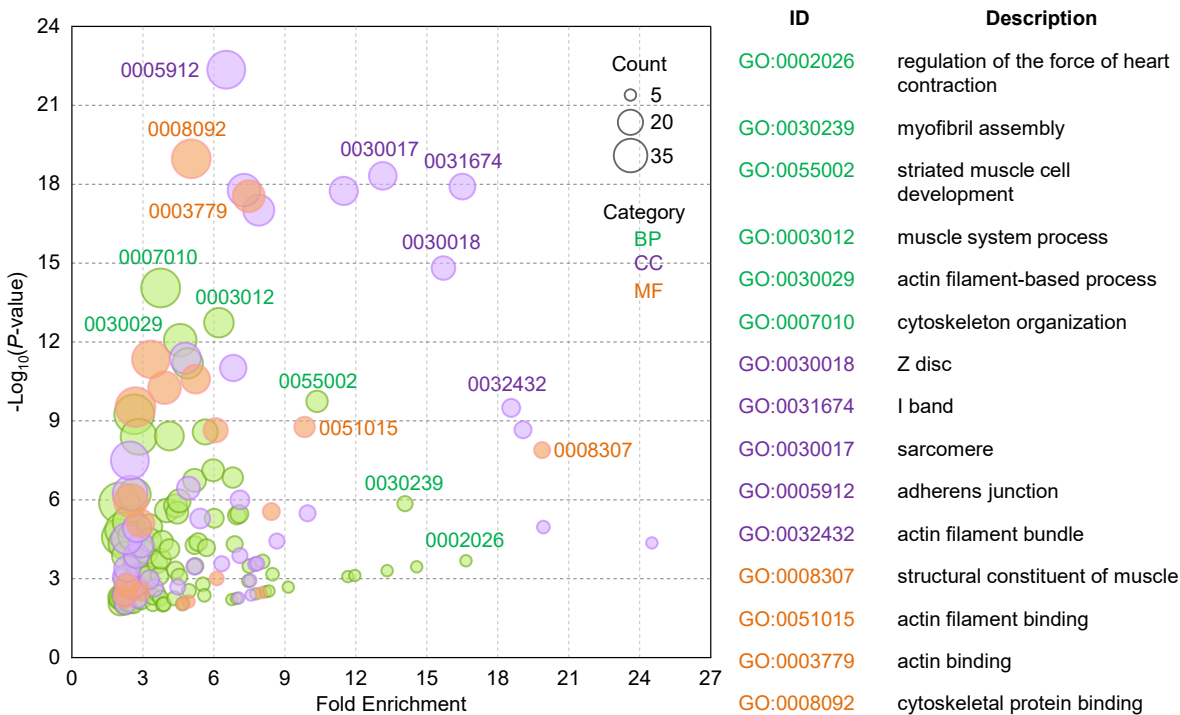




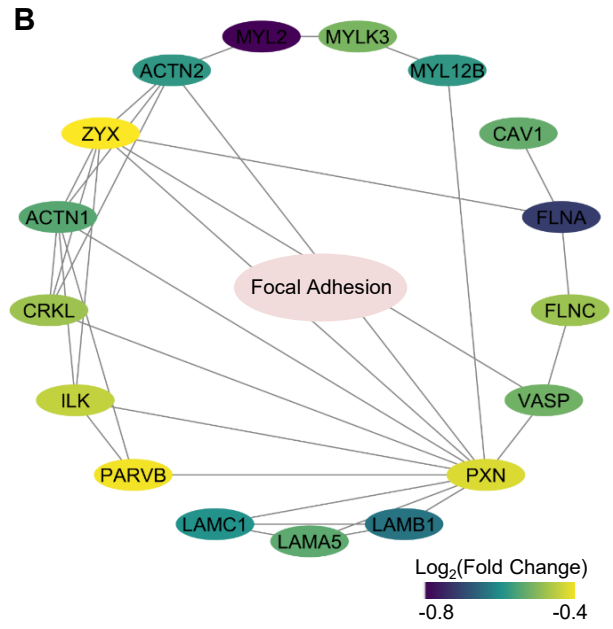
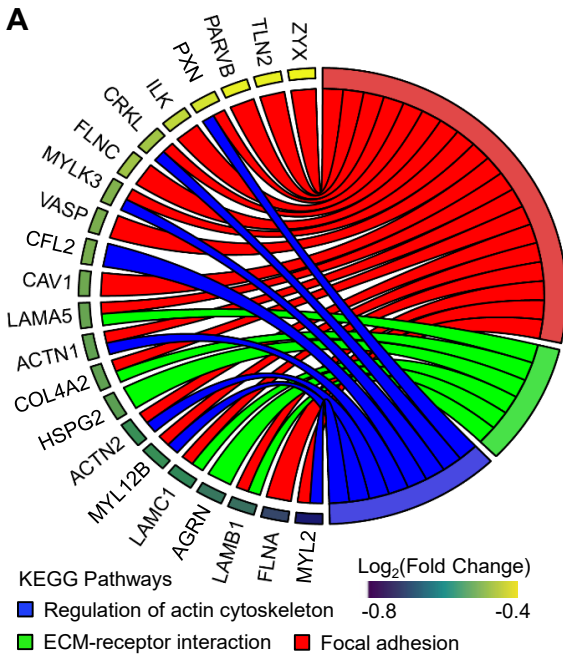
662

663

664 Figure 3



666 Figure 4



667

668